RSC Advances

PAPER

View Article Online
View Journal | View Issue

Cite this: *RSC Adv.*, 2019, **9**, 9075

Room-temperature solution synthesis of $ZnMn_2O_4$ nanoparticles for advanced electrochemical lithium storage†

Chunhui Wang,‡[a] Chunxian Zhou,‡[a] Bao Zhang,[a] Xing Ou,*[a] Liang Cao,[a] Chunli Peng[b] and Jiafeng Zhang[a]

Received 22nd January 2019
Accepted 11th March 2019

DOI: 10.1039/c9ra00553f

rsc.li/rsc-advances

Taking advantage of synergistic effects, the ternary metal oxides have attracted tremendous interest. Herein, $ZnMn_2O_4$ nano-particles have been fabricated *via* a facile one-step approach at room temperature, that of simply mixing ZnO and MnO in KOH aqueous solution without templates. When used as an anode for lithium ion batteries, it delivers the excellent structure stability (1028.9 mA h g^{-1} at 1.0 A g^{-1} after 400 cycles). Surprisingly, the low-cost and eco-friendly route provides a novel strategy to synthesize the mixed transition metal oxide electrodes with readily scaled-up production.

Presently, the energy density of lithium-ion batteries (LIBs) needs urgently to be improved to meet the market development, which is principally restricted by the current commercial graphite anode materials (≈372 mA h g^{-1}).[1,2] Hence, enormous efforts have been implemented to exploit anode materials with high capacity, such as metal oxide/sulfide,[3–5] phosphide,[6] Si-based compounds.[7] In consideration of their nontoxicity, low cost and high energy density, transition metal oxides (TMOs) have attracted extraordinary attention, owing to their high theoretical reversible capacity, which is twice as high as that of graphite.[8–10] Especially for ternary TMOs, they are considered as the most promising candidates for LIBs owing to their higher electrochemical activity and better ion/electron conductivity induced by their synergistic effects, compared with their corresponding single metal oxides.[11,12]

Among the numerous ternary TMOs, $ZnMn_2O_4$ are particularly attractive and extensively investigated, as it can offer richer redox reactions and display a relatively lower delithiation potential of 0.5 V than those of single-component oxides *vs.* Li/Li^+ (ZnO, 1.2 V and MnO, 1.5 V).[13,14] However, $ZnMn_2O_4$ will suffer from the unavoidable volume expansion, resulting in the detrimental structural collapse upon long-term lithiation/delithiation process.[15] Generally, preparing the nano-size electrode is an effective approach to mitigate the intrinsical issue, which can enhance the electrochemical performance and stabilize the microstructure. While the achievement of nanostructured materials is heavily depended on the synthetic methods. For instance, flower-like $ZnMn_2O_4$ is synthesized by solvothermal process, and it displays an initial charge capacity of about 763 mA h g^{-1} and retains stable performance after 50 cycles.[16] One-dimensional $ZnMn_2O_4$ nanowires have been fabricated by mixing α-MnO_2 and $Zn(CH_3COO)_2$ under high temperature calcination at 480 °C in O_2 atmosphere. However, the synthesis procedure introduces the template of precursor of α-MnO_2 nanowires, which are complicated to obtain by hydrothermal approach.[17] Besides, the ball-in-ball hollow microspheres of $ZnMn_2O_4$ electrode can only be manufactured by liquid phase method with reflux condensation and post-thermal treatment.[18] Unfortunately, although the nanosized $ZnMn_2O_4$ prepared by the above studies deliver a good electrochemistry property, the operational process is fairly complex and the productivity is relatively low, hindering the further development of $ZnMn_2O_4$ anodes. Therefore, it is urgent to explore a novel and highly efficient synthetic method to fabricate nanosized $ZnMn_2O_4$ with improved electrochemical performance.

Herein, one-step room-temperature synthesis of $ZnMn_2O_4$ nano-particles based on facile KOH solution system and low-cost precursor materials has been designed and presented in this investigation. The synthesized $ZnMn_2O_4$ anode exhibits satisfied electrochemical properties in regard of high reversible capacity and excellent cycling stability. Compared with previously reported $ZnMn_2O_4$ materials synthesized at elevated temperature, it is facile, up-scalable and high-efficient for our work, which provide a new strategy to realize the large fabrication of other TMOs, such as $ZnFe_2O_4$, $ZnCo_2O_4$.

The $ZnMn_2O_4$ nano-particles were synthesized through a facile, low cost route in one-step process, which is depicted in

[a]*School of Metallurgy and Environment, Central South University, Changsha 410083, PR China. E-mail: ouxing@csu.edu.cn*

[b]*School of Energy Science and Engineering, Central South University, Changsha 410083, PR China*

† Electronic supplementary information (ESI) available: Experimental section, material characterizations, electrochemical characterizations, Fig. S1–S5. See DOI: 10.1039/c9ra00553f

‡ These authors contributed equally and mainly to this study.

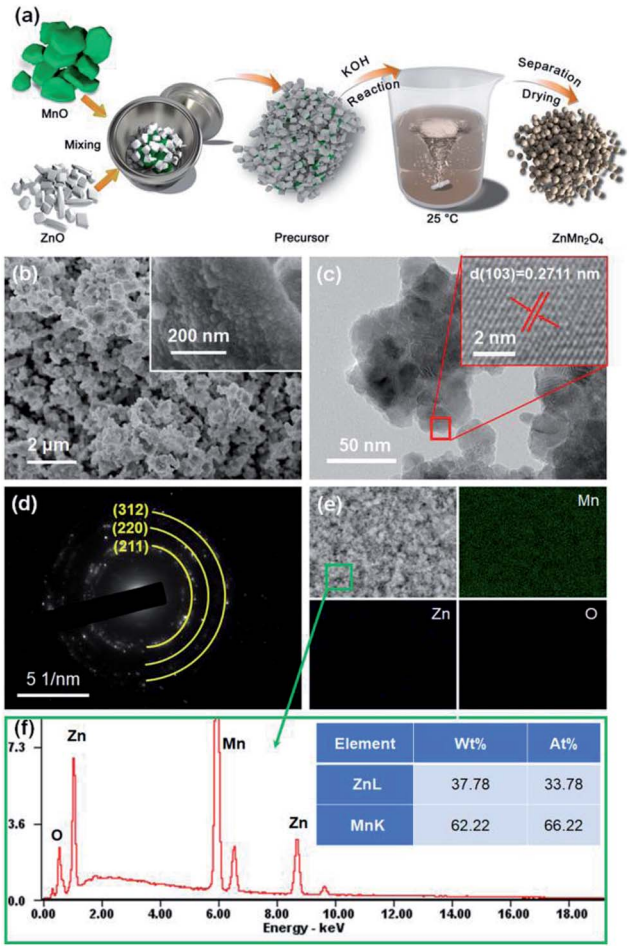

Fig. 1 (a) The schematic illustration of the fabrication procedure of $ZnMn_2O_4$; the SEM (b), TEM (c), SAED pattern (d), mapping profile (e) and the EDS spectroscopy pattern (f).

Fig. 1a. In the basic medium of KOH aqueous solution, MnO could be slowly oxidized to Mn_3O_4 (Fig. S3†) by O_2. Meanwhile, with the presence of the Zn^{2+}, the $ZnMn_2O_4$ could be prepared at same time in oxidization.[19] As displayed in the SEM image of $ZnMn_2O_4$ materials (Fig. 1b), the nano-sized particles with dimension of 20–30 nm get aggregation into bulk morphology, which is obviously different from the pristine samples (Fig. S1†) and is also confirmed by TEM (Fig. 1c). Predictably, after mixing the precursors in the solution process, the $ZnMn_2O_4$ materials are synthesized, which indicate that the approach is feasible and is confirmed by the following measurements of HRTEM and XRD. From the HRTEM image (inset of Fig. 1c), it can be clearly observed the interplanar spacing of 0.271 nm, well matching with the (103) planes of $ZnMn_2O_4$ phase, indicating the high crystallization of as-prepared $ZnMn_2O_4$. Moreover, the corresponding SAED pattern (Fig. 1d) is well indexed to the crystal planes of (211), (220), and (312) of $ZnMn_2O_4$, demonstrating the polycrystalline characters by the clear diffraction rings. The elemental mapping images (Fig. 1e) ascertains that the electrode is consisted of Zn, Mn and O with evenly distributed, and the molar ratio of Zn and Mn is approaching 1 : 2 (Fig. 1f), confirming the formation of $ZnMn_2O_4$.

The XRD pattern of the $ZnMn_2O_4$ nanoparticles is shown in Fig. 2a, which can be well indexed into the tetragonal structure of $ZnMn_2O_4$ with a space group of $I4_1/amd$ (141) (JCPDS no. 24–1133). Meanwhile, as presented in the Raman spectra (Fig. 2b), it exhibits three obvious peaks located at 326, 369 and 671 cm^{-1}, which is consistent with the typical vibration modes of $ZnMn_2O_4$.[20] The peak at 671 cm^{-1} is corresponding to the oxygen motion in the tetrahedral AO_4 group with A_{1g} symmetry, and the other two modes are characteristic of the octahedral site (BO_6).[21] The valence state and chemical composition are analysed by XPS (Fig. 2c and d). The full spectrum displays four elements, Zn, Mn, O, and C in Fig. 2c and S3,† and the C 1s spectrum (282.8 eV) is assigned to carbonate materials existed in the XPS instrument. The Mn 2p peak can be split into two peaks at 653.4 and 641.7 eV with an energy margin of 11.7 eV, associated to the Mn $2p_{1/2}$ and $2p_{3/2}$, respectively, which confirms the oxidation state of Mn^{3+} in the $ZnMn_2O_4$ nanoparticles.[22,23]

To evaluate the lithium storage performance of $ZnMn_2O_4$, various electrochemical measurements were conducted as anodes in the coin cells. Cyclic voltammetry (CV) test at a rate of 0.1 mV s^{-1} in potential range of 0.01–3.0 V is employed to explore the lithium-ion reaction mechanism of $ZnMn_2O_4$, as shown in Fig. 3a. During the initial cathodic sweep, the first occurred peak at 1.08 V is consistent to the reduction from Mn^{3+} to Mn^{2+}, and the following peak located at 0.75 V is ascribed to the electrolyte decomposition accompanied with the formation of the solid electrolyte interphase (SEI), respectively, which disappears in the subsequent scans. Meanwhile, the peak at 0.41 V is assigned to the irreversible reduction reaction of Mn^{2+} and Zn^{2+} into Zn^0 and Mn^0 embedded in amorphous Li_2O matrix. While the peak at low potential (about 0.08 V) is corresponding to the formation of Li–Zn alloy (Fig. S6†), which is consistent with the earlier CV profiles.[16] In the corresponding anodic scan, two oxidation peaks at approximately 1.2 and 1.5 V are associated to the reversible oxidation of Zn^0 and Mn^0, and

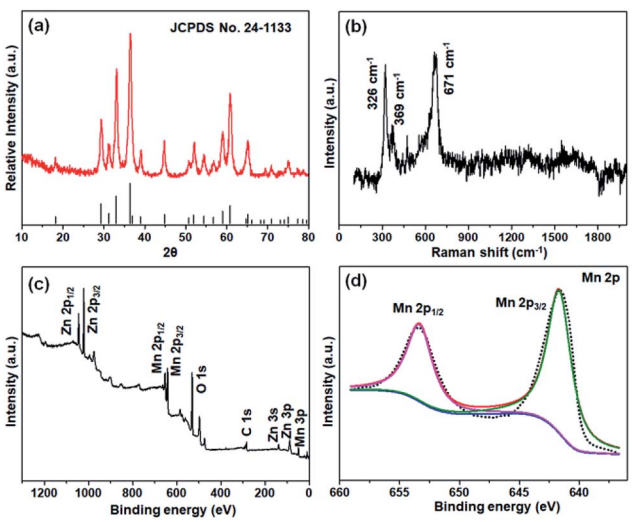

Fig. 2 The results of XRD (a), Raman spectra (b), XPS full spectrum (c) and the high-resolution spectrum of Mn 2p (d).

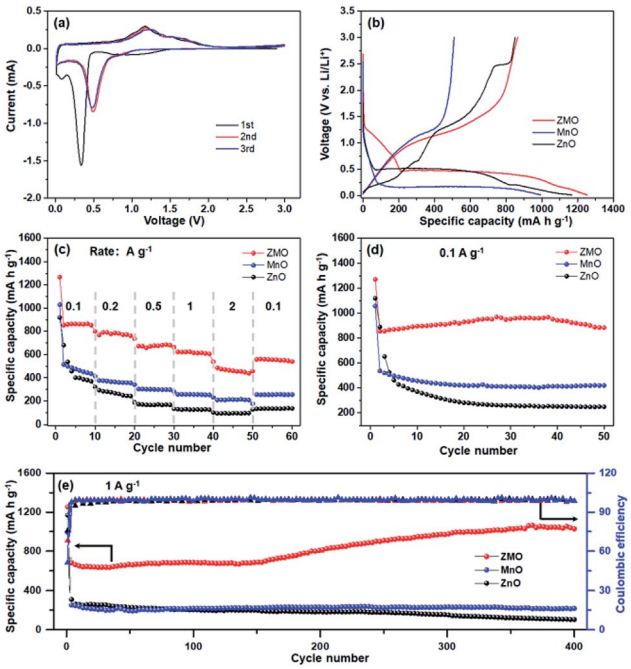

Fig. 3 (a) The *CV* curves of $ZnMn_2O_4$ electrode at a scan rate of 0.1 mV s^{-1} between 0.01 V and 3 V. (b) Charge–discharge profiles for the first cycle at a current of 0.1 A g^{-1}, (c) the rate property at different rates, the cycling performance at 0.1 A g^{-1} (d) and 1 A g^{-1} (e) for all the samples.

formation of ZnO and MnO, respectively.[24,25] In the following scans, the reduction peak for conversion reaction shifts from 0.41 V to 0.49 V, ascribing to the small overpotentials induced by smaller particles.[22] Furthermore, the following CV profiles almost completely superimposed for each other, suggesting the excellent reversibility and stability of $ZnMn_2O_4$ anode.

The first discharge–charge curves of $ZnMn_2O_4$ nano-particles (abb. ZMO) and precursor materials (ZnO and MnO) are shown in Fig. 3b, recorded at 0.1 A g^{-1} in the potential range of 0.01–3.0 V. The as-prepared $ZnMn_2O_4$ shows a voltage plateau at 0.43 V, which is in accordance with the CV profiles. While it displays an initial charge capacity of 865.6 mA h g^{-1} with an acceptable coulombic efficiency (70.1%), higher than those of the ZnO (851.6 mA h g^{-1}) and MnO (509.8 mA h g^{-1}). The rate capability of $ZnMn_2O_4$ is demonstrated in Fig. 3c. The $ZnMn_2O_4$ anode delivers 863.4, 781.9, 676, 622.7 and 470 mA h g^{-1} at rate increasing from low current to ultrahigh (0.1, 0.2, 0.5, 1.0 and 2.0 A g^{-1}). When returned back to 0.1 A g^{-1}, it immediately recovered to 555.6 mA h g^{-1}, much higher than that of pristine ZnO and MnO samples, indicating their advanced kinetic properties. The cycling performance of $ZnMn_2O_4$ is also superior compared with pristine ZnO and MnO. It is noteworthy that $ZnMn_2O_4$ shows the reversible capacity of 884.5 mA h g^{-1} after 50 cycles at rate of 0.1 A g^{-1} (Fig. 3d). Furthermore, it maintains a reversible capacity of 1028.9 mA h g^{-1} after 400 cycles at rate of 1 A g^{-1}, equivalent to capacity retention of 82.08%. Interestingly, it suffers from capacity loss during the initial dozens of cycles, but thereafter, it begins to increase significantly, which is normally found in other TMO-material anodes. This phenomenon is generally attributed to the polymeric gel-like

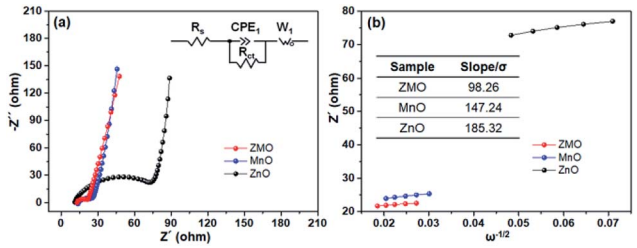

Fig. 4 (a) The EIS spectra of all samples and the equivalent electrical circuit (inset), (b) the liner fitting of Z' *vs.* $\omega^{-1/2}$ in the low-frequency and the value of σ (inset).

film with continuous and reversible formation during the kinetic activation process of anode.[18,26]

The EIS profiles of the three samples are Nyquist plots, fitted by the corresponding equivalent circuit as displayed inset of Fig. 4a. The charge-transfer resistance is noted as R_{ct} and Li^+ diffusion coefficient is calculated as followed:[27,28]

$$D = (R^2T^2)/(2A^2n^4F^4C^2\sigma^2) \quad (1)$$

Herein, R, T, A, n, F, and C are attributed to the gas constant, absolute temperature, area of electrode, electrons number, Faraday constant, and concentration of Li^+, respectively. Furthermore, σ represents the Warburg impedance coefficient, which is associated with Z':

$$Z' = R_s + R_{ct} + \sigma\omega^{-1/2} \quad (2)$$

Where the R_s and ω are ohmic resistance and angular frequency, respectively.[23] The R_{ct} value of $ZnMn_2O_4$ (8.61 Ω) is lower than that of ZnO (66.69 Ω) and MnO (12.33 Ω) and the D value is higher than that of others ($D_{ZMO} = 2.87 \times 10^{-12}$, $D_{ZnO} = 8.07 \times 10^{-13}$, $D_{MnO} = 1.28 \times 10^{-12}$), which is consistent with the analysis of the cycling and rate performance. This enhanced inherent kinetics can be assigned to the shortened distance for Li-ion diffusion, resulting from the characteristic of nanosized particles. While the ternary oxide can facilitate electron transport in contrast to the individual oxide induced by the synergistic effect.

In summary, nano-particles $ZnMn_2O_4$ with high yields were synthesized by a facile solution reaction route without template at room temperature. Unlike other materials for amorphous state, the as-prepared $ZnMn_2O_4$ exhibits strong crystalline with a nanostructure morphology. Electrochemical measurements demonstrate that the as-prepared $ZnMn_2O_4$ exhibits remarkable reversible capacity and cycling stability, superior to those of pristine materials. The facile strategy opens up a new approach to fabricate ternary or multiphase transition metal oxides at room temperature, which can promote the development and keep highly promising to scale-up of transition metal oxides as anodes for LIBs.

Conflicts of interest

There are no conflicts to declare.

Acknowledgements

This study was supported by National Natural Science Foundation of China (Grant No. 51772334, 51778627 and 51822812).

Notes and references

1 C. Zhu, R. E. Usiskin, Y. Yu and J. Maier, *Science*, 2017, **358**, easo2808.
2 S. Wei, S. Choudhury, Z. Tu, K. Zhang and L. A. Archer, *Acc. Chem. Res.*, 2018, **51**, 80–88.
3 C. J. Heard, J. Čejka, M. Opanasenko, P. Nachtigall, G. Centi and S. Perathoner, *Adv. Mater.*, 2018, 1801712.
4 X. Chia and M. Pumera, *Chem. Soc. Rev.*, 2018, **47**, 5602–5613.
5 W. H. Ren, D. N. Liu, C. L. Sun, X. H. Yao, J. Tan, C. M. Wang, K. N. Zhao, X. P. Wang, Q. Li and L. Q. Mai, *Small*, 2018, **14**, 1800659.
6 M. Sun, H. Liu, J. Qu and J. Li, *Adv. Energy Mater.*, 2016, **6**, 1600087.
7 H. Shang, Z. Zuo, L. Yu, F. Wang, F. He and Y. Li, *Adv. Mater.*, 2018, **30**, e1801459.
8 M. V. Reddy, G. V. Subba Rao and B. V. Chowdari, *Chem. Rev.*, 2013, **113**, 5364–5457.
9 C. Yuan, H. B. Wu, Y. Xie and X. W. Lou, *Angew. Chem., Int. Ed.*, 2014, **53**, 1488–1504.
10 Y. Zhao, L. P. Wang, M. T. Sougrati, Z. Feng, Y. Leconte, A. Fisher, M. Srinivasan and Z. Xu, *Adv. Energy Mater.*, 2017, **7**, 1601424.
11 Y. Sharma, N. Sharma, G. V. Subba Rao and B. V. R. Chowdari, *Electrochim. Acta*, 2008, **53**, 2380–2385.
12 L. Q. Mai, F. Yang, Y. L. Zhao, X. Xu, L. Xu and Y. Z. Luo, *Nat. Commun.*, 2011, **2**, 381–384.
13 Y. Deng, S. Tang, Q. Zhang, Z. Shi, L. Zhang, S. Zhan and G. Chen, *J. Mater. Chem.*, 2011, **21**, 11987–11995.
14 Q. Gao, Z. Yuan, L. Dong, G. Wang and X. Yu, *Electrochim. Acta*, 2018, **270**, 417–425.
15 M. H. Alfaruqi, A. K. Rai, V. Mathew, J. Jo and J. Kim, *Electrochim. Acta*, 2015, **151**, 558–564.
16 L. F. Xiao, Y. Y. Yang, J. Yin, Q. Li and L. Z. Zhang, *J. Power Sources*, 2009, **194**, 1089–1093.
17 S.-W. Kim, H.-W. Lee, P. Muralidharan, D.-H. Seo, W.-S. Yoon, D. K. Kim and K. Kang, *Nano Res.*, 2011, **4**, 505–510.
18 G. Zhang, L. Yu, H. B. Wu, H. E. Hoster and X. W. Lou, *Adv. Mater.*, 2012, **24**, 4609–4613.
19 B. G. S. Raj, A. M. Asiri, J. J. Wu and S. Anandan, *J. Alloy. Compd.*, 2015, **626**, 234–240.
20 J. G. Kim, S. H. Lee, Y. Kim and W. B. Kim, *ACS Appl. Mater. Interfaces*, 2013, **5**, 11321–11328.
21 T. Zhang, H. Yue, H. Qiu, K. Zhu, L. Zhang, Y. Wei, F. Du, G. Chen and D. Zhang, *RSC Adv.*, 2015, **5**, 99107–99114.
22 X.-F. Chen, L. Qie, L.-L. Zhang, W.-X. Zhang and Y.-H. Huang, *J. Alloy. Compd.*, 2013, **559**, 5–10.
23 L. Huang, Y. Huang, J. Liang, X. Wan and Y. Chen, *Nano Res.*, 2011, **4**, 675–684.
24 H. Rong, G. Xie, S. Cheng, Z. Zhen, Z. Jiang, J. Huang, Y. Jiang, B. Chen and Z.-J. Jiang, *J. Alloy. Compd.*, 2016, **679**, 231–238.
25 Z. Bai, N. Fan, C. Sun, Z. Ju, C. Guo, J. Yang and Y. Qian, *Nanoscale*, 2013, **5**, 2442–2447.
26 L. Hou, L. Lian, L. Zhang, G. Pang, C. Yuan and X. Zhang, *Adv. Funct. Mater.*, 2015, **25**, 238–246.
27 L. Cao, B. Zhang, X. Ou, C. Wang, C. Peng and J. Zhang, *Small*, 2019, **15**, 1804861.
28 C. Shen, H. Long, G. Wang, W. Lu, L. Shao and K. Xie, *J. Mater. Chem. A*, 2018, **6**, 6007–6014.